




Immobilized Mo:TiO₂ nanoparticles for humic acid removal in an aqueous medium using solar spectrum

Kamaladdin Abedi¹, Behzad Shahmoradi^{2,*}, Kitirote Wantala³, Totsaporn Suwannaruang³, Nader Amini⁴, Afshin Maleki², S. M. Lee⁵, and Harikaranahalli Puttaiah Shivaraju^{6,*} 

¹Department of Occupational Health Engineering, Faculty of Health, Kurdistan University of Medical Sciences, Sanandaj, Iran

²Department of Environmental Health Engineering, Faculty of Health, Kurdistan University of Medical Sciences, Sanandaj, Iran

³Department of Chemical Engineering, Faculty of Engineering, Khon Kaen University, Khon Kaen, Thailand

⁴Environmental Health Research Center, Research Institute for Health Development, Kurdistan University of Medical Sciences, Sanandaj, Iran

⁵Department of Health and Environment, Catholic Kwandong University, Gangnung 25601, Republic of Korea

⁶Department of Environmental Sciences, JSS Academy of Higher Education and Research, Sri Shivarathreshwara Nagara, Mysuru, Karnataka 570015, India

Received: 1 February 2022

Accepted: 7 June 2022

Published online:
17 June 2022

© The Author(s), under exclusive licence to Springer Science+Business Media, LLC, part of Springer Nature 2022

ABSTRACT

The presence of humic acids and their compounds react with chlorinated residues during water disinfection processes and produce toxic halogenated hydrocarbons, which are carcinogenic. The aim of this research work was to determine photocatalytic degradation of humic acid in an aqueous media using molybdenum-doped titanium dioxide nanoparticles (Mo:TiO₂ NPs) under the visible light spectrum. Mo:TiO₂ nanomaterials were synthesized through mild hydrothermal techniques and characterized through powder XRD, SEM, DLS, and XPS. The effect of operational parameters including dopant percentage, the dosage of photocatalyst, contact time, and concentration of humic acid was investigated and optimized in the degradation process. Characterization results showed spherically shaped well crystalline-structured nanoparticles that enhance the photocatalytic activities. Among the nanomaterials, 1% Mo:TiO₂ nanomaterials showed the highest degradation efficiencies up to 83%; however, the optimum conditions for the highest efficiency obtained for immobilized Mo:TiO₂ NPs are different from slurry mode.

Address correspondence to E-mail: bshahmorady@gmail.com; shivarajuenvi@gmail.com

1 Introduction

Natural organic matter (NOM) is formed as a result of the biological and chemical decomposition of plants and animal components in aquatic environments [1]. These compounds are classified into two groups: hydrophilic and hydrophobic. Hydrophilic compounds such as carboxylic acids, carbohydrates, and proteins. Humic and fulvic materials (containing aromatic rings, phenolic rings, and binary bonds), on the other hand, are examples of hydrophobic NOMs. Chemists have divided humic substances into three groups depending on their solubility in an aqueous medium: (I) the first group and the most important are humic acids, which are completely insoluble, (II) the second group consists of haloacetic acids, which are soluble in alkaline pH and are insoluble in acidic medium, and (III) the third group consists of fulvic acids, which are soluble in either acidic or basic media [2]. Humic substances typically make up 60 to 90% of the total NOMs of aquatic systems [3]. Humic acid has been identified in varying amounts in water sources and can have adverse effects on the ecosystem; hence, much research works have focused on removing these compounds from aquatic environments [4–7]. Humic compounds in water treatment processes such as chlorine disinfection create by-products such as haloacetic acid (HAA) and trihalomethanes (THM), both of which are toxins and can cause kidney problems, bladder damage, and cancer or mutagenesis [8, 9]. The Environmental Protection Agency (EPA) recommends HAA and THM concentrations in drinking water of 60 and 80 mg/l, respectively. Apart from by-products, humic compounds can cause the growth of microorganisms and algae in water distribution tanks and pipelines and cause problems in their taste, color, and odor, adsorb impurities such as hazardous heavy metals from water sources, and transfer these impurities to the water resources. Therefore, it is recommended to use appropriate methods to remove these compounds from water sources before their disinfection by chlorine and discharge into water bodies [2, 4, 6].

Processes such as adsorption, coagulation, sedimentation, filtration, and chemical and membrane processes are used to remove various water contaminants [10, 11]. Each of the mentioned methods has many disadvantages in terms of sludge production, economic efficiency, treatment speed, and

ability to remove various pollutants. The low efficiency of the mentioned methods in removing organic and toxic compounds in industrial wastewater has necessitated the use of more efficient methods. Advanced oxidation processes (AOPs) are one of the most efficient methods of degrading organic compounds. AOPs refer to the processes in which OH radicals with high reactivity are produced for the effective treatment of wastewater. By performing the oxidation process, organic matter is converted into minerals and finally, the amount of pollution is reduced [12–14]. Among the AOPs, the photocatalytic process is highly effective in degrading compounds and converting harmful pollutants into carbon dioxide, water, and minerals [10]. Various nanophotocatalysts, such as Fe_2O_3 , CuO , Fe_3O_4 , SiO_2 , rGO, WO_3 , and TiO_2 , are used to perform photocatalytic processes [15–21], G. [22]. Titanium dioxide is the most commonly used photocatalyst, which has received a lot of attention due to its easy availability, relatively cheap price, the possibility of simple laboratory preparation, and high stability [23]. However, titanium dioxide has some drawbacks such as a high band gap (3.2 eV) [24], which makes it inefficient in visible light and its main activity is done in UV light [23]. Given that UV makes up only 4% of sunlight and visible light about 44 to 47% of sunlight [25, 26], hence it is necessary to modify TiO_2 using compounds that increase light absorbance and change the absorption from the UV region to the visible region [23]. Doping TiO_2 with suitable dopants changes the energy band gap and increases its effect on the photodegradation of organic and toxic pollutants. However, doping nanoparticles with a suitable metal cannot solve the problems of agglomeration and poor dispersion of semiconductor nanoparticles; hence, to overcome this problem, suitable low toxicity, low density, low melting point, and decomposable surfactants could be used [27]. Molybdenum oxide is a metal oxide that has a smaller ionic radius and energy gap than TiO_2 [28]. Therefore, it is a suitable candidate as a titanium dioxide dopant [29]. Moreover, doping TiO_2 with Mo can create an n–n heterogeneous structure and the modified catalyst has a higher photocatalytic mineralization capacity and effectively introduces external defects due to its unique configuration and ionic radius similar to Ti^{4+} and increases its photocatalytic properties [30]. Based on the latest available literature, the photodegradation of humic substances has not been studied using

immobilized Mo:TiO₂ nanoparticles. Therefore, the use of sandblasted glass as a substrate might increase the photodegradation efficiency of humic materials due to the immobilization of Mo:TiO₂ nanoparticles. Moreover, the effect of operational parameters including the concentration of humic substances, contact time, and dosage of Mo:TiO₂ nanoparticles was evaluated.

2 Materials and methods

2.1 Chemicals

Technical and analytical grade humic acid was purchased from Sigma-Aldrich (USA). Other chemicals including NaOH, TiO₂, MoO₂, and HCl were purchased from Hack (Germany) and used without any change.

2.2 Hydrothermal synthesis of Mo:TiO₂ nanoparticles

Mo:TiO₂ nanoparticles were synthesized through the mild hydrothermal method. In Brief, firstly 1 mol of TiO₂ and different weight percentages (0.5, 1.0, and 1.5%) of MoO₂ were added to a Teflon liner and mixed by gently adding 10 ml 1 mol NaOH as solvent. To the mixture, 1 ml of *n*-butylamine was added dropwise and mixed using a glass rod for several minutes until a uniform and homogeneous solution was obtained. The liner was packed and placed in a General purpose autoclave. After sealing the autoclave, it was kept in an oven for 12 h at 120 °C. After quenching the autoclave, as the initial pH was not too high (pH = 8.3 ± 0.2), the content was centrifuged at 4000 rpm for 2 min several times using fresh double distilled water as the solvent until the pH of the content became neutral. Then the nanoparticles were dried at 60 °C for 24 h. The final nanoparticles were kept in the desiccator until systematic characterization and photocatalytic studies [31].

2.3 Immobilization of Mo:TiO₂ nanoparticles fabricated

Several glass plates with dimensions of 3 × 12 cm were used for fixing the nanoparticles on them. First, the surface of the glass was sandblasted to increase

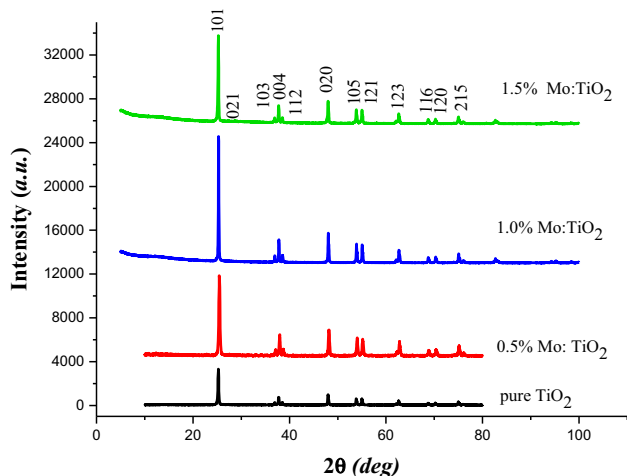
the chance of coating the particles on it. Then, to activate the surface of the sandblasted glasses for better stabilization, each glass was placed in concentrated NaOH for 24 h. After taking the sandblasted glasses from the solution, they were washed with deionized water to neutral pH. The glasses were later dried at room temperature. The homogeneous suspension of 1 wt% of Mo:TiO₂ was evenly coated on the glass surface using a 5 ml pipette. The suspension was variable in terms of the concentration of nanoparticles dissolved in water, so concentrations of 0.5, 1, 2, and 3 g/100 ml of distilled water were used. They were then dried at room temperature for 24 h. Finally, the coated sandblasted glasses were placed in an oven at 450 °C for 3 h for calcination [32].

2.4 Characterization studies of Mo:TiO₂ nanoparticles

The materials fabricated were characterized using SEM image (Model FE-SEM SU-70, Hitachi, Japan) and FE-SEM (MIRA III, TESCAN, Czech Republic), and XRD (Model X'Pert PROMPD, PANalytical, the Netherlands) measurements were conducted using the Cu K_{a1} and K_{a2} wavelengths 1.54060 and 1.54443 Å, respectively, having the generator settings at 30 mA and 40 kV. The measurements were made using 0.020° per step and at a time step of 2.8 s. Further, the valence states of each element were studied by X-ray photoelectron spectroscopy (XPS), (K-ALPHA + XPS System, Thermo Fisher Scientific with Al K_α X-ray source ($h\nu = 1486.6$ eV)). DLS (NANOBROOK, Brookhaven, USA) was used for determining the size distribution of the nanoparticles synthesized. A solution of 10 mg/l Mo:TiO₂ was prepared in either ultrapure water (18.2 MΩ cm) or unfiltered stream water (pH 8.12) and then filtered stream water (0.22-μm PTFE membrane). Immediately after adding the Mo:TiO₂ to water, the samples were shaken vigorously and 3 ml was added to a plastic cuvette for DLS measurement. All measurements were conducted at a 90° scattering angle at 25 °C with a 10-s equilibration time. Cell parameters of Mo:TiO₂ nanoparticles were calculated using ChekCell Shareware.

Table 1 Cell parameters of Mo:TiO₂ nanoparticles

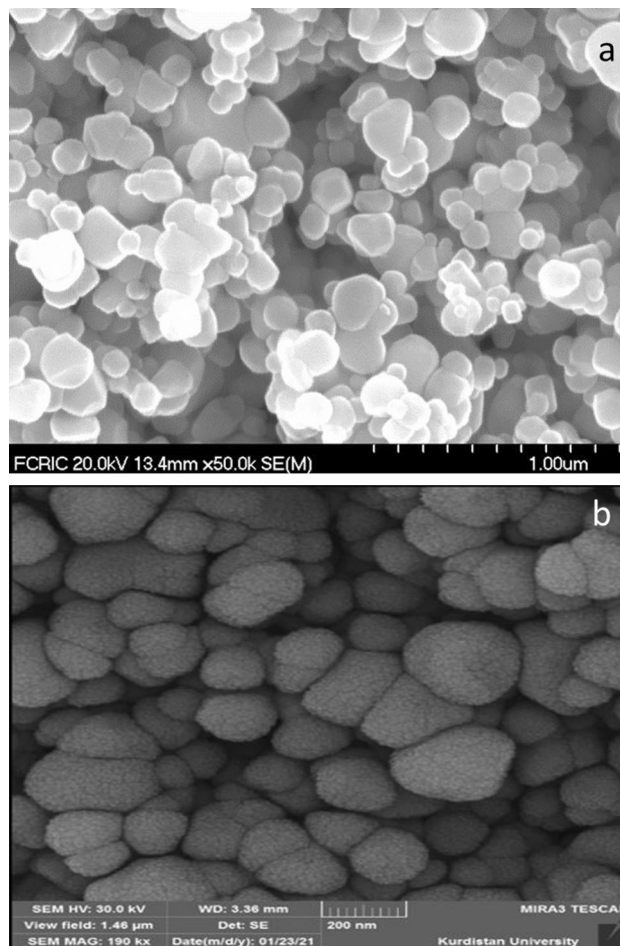
Dopant percentage	<i>a</i> (Å)	<i>C</i> (Å)	<i>a/c</i> ratio	<i>V</i> (Å ³)
0.0	3.7845	9.5143	0.3977	136.30
0.5	3.7878	9.5114	0.3982	136.46
1.0	3.7886	9.5104	0.3983	136.51
1.5	3.7902	9.5112	0.3984	136.63

**Fig. 1** Powder XRD patterns of pure TiO₂ and different wt% Mo:TiO₂ nanoparticles

2.5 Photocatalytic assessment of humic acid degradation

For photocatalytic degradation experiments, a closed rectangular cubic reactor made of Plexiglas with a length of 30 cm, a width of 15 cm, and a height of 10 cm was used. Direct sunlight was applied as a free energy-driven source. We used a Lux meter (Lutron, Taiwan) to measure the light intensity and its intensity was beyond the detection limit of the instrument used for this purpose, i.e., +20,000 Lux. Each experiment was carried out from 11:00 am to 2:00 pm. From 11:00 to 12:00 was for measurement of adsorption–desorption equilibrium and related readings. The reactor was kept on a shaker ($\omega = 100$ rpm).

Various operational parameters were changed to achieve the highest degradation efficiency. The most important operational parameters were percentage of dopant (0.5, 1.0, and 1.5 wt% of Mo:TiO₂), the dosage of nanoparticles (0.5, 1, 2, and 3 g/l), concentration of humic acid (10, 25, 50, 75, 100, 150, and 200 mg/l), different modes of using nanoparticles (slurry and

**Fig. 2** SEM images of 1 wt% Mo:TiO₂ nanoparticles: **a** before and **b** after immobilization

immobilized Mo:TiO₂), and reaction time (20, 40, 60, 80, 100, 120, 140, 160, 180, and 200 min). Each experiment was performed at neutral pH. For the photodegradation study, first, the samples containing nanoparticles were kept in darkness for 30 min to check adsorption–desorption equilibrium. Then the concentration of humic acid was measured at $\lambda = 254$ nm using a spectrophotometer. The photodegradation efficiency is calculated using Eq. 1 [33].

$$R = (C_i - C_f / C_i) \times 100 \quad (1)$$

where *R* is the photodegradation efficiency in % and *C_i* and *C_f* are the initial and final concentrations of humic acid in mg/l, respectively.

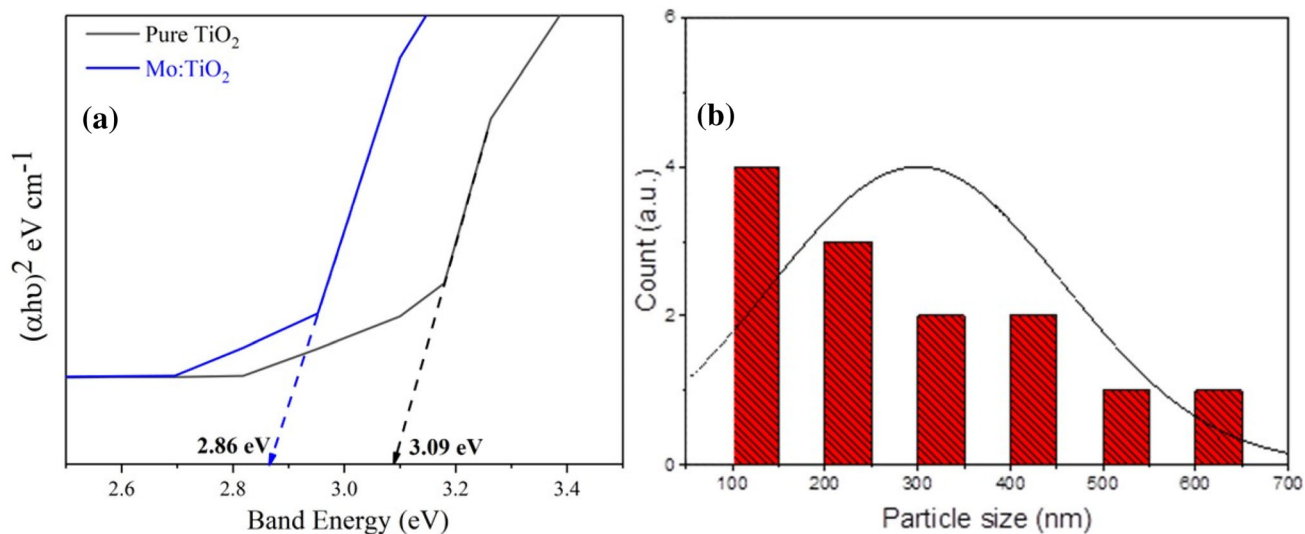


Fig. 3 **a** Band gap energy; **b** DLS of 1.0% Mo:TiO_2 nanoparticles

3 Results and discussion

3.1 Characterization of Mo:TiO_2 nanoparticles

Figure 1 shows the powder XRD pattern of bare (undoped) and Mo:TiO_2 nanoparticles. In the XRD patterns of Mo:TiO_2 nanoparticles, it was observed that all samples had an anatase structure (ICDD File number: 03-065-5714) with specific diffraction peaks corresponding to positions (101), (103), (004), (112), (020), (105), (121), (123), (116), (120), and (215), respectively. Therefore, XRD analysis indicates the synthesis of Mo:TiO_2 in the anatase phase [34, 35]. Doping TiO_2 with different percentages of molybdenum has led to the formation of a weak, low-intensity peak at position 021 in the titanium oxide structure. The reason for its weakness is the small amount of molybdenum compared to titanium oxide. Moreover, due to the proximity of the ionic radii of TiO_2 and Mo and the consequent replacement of Mo ions in the TiO_2 structure, no additional peak can be displayed, indicating that this method is an easy method for the synthesis of existing nanoparticles [36]. In addition, the sharp peaks shown in the XRD pattern indicate the good crystallization of Mo:TiO_2 nanoparticles [37]. Moreover, the cell parameters of Mo:TiO_2 nanoparticles with different dopant percentages are tabulated in Table 1. The comparison of cell parameters shows that the cell volume increased as the dopant percentage increases. Such a trend could be

attributed to the ionic radius of Mo (0.69 nm), which is higher than Ti (0.42 nm) [32].

SEM analysis was performed to investigate the surface morphology and determine the size of the synthesized samples as shown in Fig. 2. Figure 2a shows the SEM image of powder 1 wt% Mo:TiO_2 nanoparticles (before immobilization) having spherical shapes revealing the effect of the surfactant used over the morphology of the nanoparticles fabricated. Figure 2b shows the SEM image of immobilized 1 wt% Mo:TiO_2 nanoparticles having a regular arrangement and uniform distribution of the nanoparticles on the sandblasted glass surface. Figure 3a shows the band gap energy of 1 wt% Mo:TiO_2 nanoparticles and it indicates the considerable reduction of band gap energy up to 2.86 eV toward the visible spectrum activation when compared to pure TiO_2 (3.09 eV). The results confirmed the activation of photocatalytic nanomaterials under visible range that provides an opportunity to treat various pollutants under natural sunlight as alternative driving energy. DLS characterization results confirmed the particles distribution at the nanoscale and DLS results can be seen in Fig. 3b.

The XPS analysis of 1.0% Mo:TiO_2 nanoparticles was characterized to investigate the valence state of Mo, Ti, and O atoms in the sample. The results are provided in Fig. 4. The wide-scale XPS spectra of 1.0% Mo:TiO_2 nanoparticles are displayed in Fig. 4a. As seen, the peaks of C 1s, O 1s, Ti 2p, and Mo 3d were obtained in 1.0% Mo:TiO_2 nanoparticles. The

binding energy of C 1s (284.6 eV) was used to calibrate the electron binding energies of each element. The valence state properties of respective elements in the samples obtained from the high-resolution XPS spectra of Ti 2*p*, O 1*s* and Mo 3*d* with the help of Gaussian fitting were explained as follows. The deconvoluted Ti 2*p* spectrum, as represented in Fig. 4b, displayed the main peaks at binding energies of 458.5 and 464.3 eV, which fitted to the Ti 2*p*_{3/2} and Ti 2*p*_{1/2} of Ti⁴⁺ in the TiO₂ lattice [30, 38–40]. Surprisingly, the Ti 2*p* peak of binding energy at 459.6 eV was also observed, which can be ascribed to the small amount of Ti³⁺ present in the TiO₂ crystal [40–42] Fig. 4c reveals the O 1*s* XPS spectra of 1.0% Mo:TiO₂ nanoparticles. The O 1*s* spectrum can be

deconvoluted into two symmetrical peaks. According to the literature, the main peak at 529.8 eV is referred as to O²⁻ in the TiO₂ lattice, while the lower peak at 530.8 eV can be assigned to the non-lattice oxygen presented as the –OH group due to chemisorption of H₂O [30, 38–40]. The Mo 3*d* electron core-level XPS spectrum is shown in Fig. 4d, the peaks can be indicated at 232.7 and 235.8 eV, representing Mo 3*d*_{5/3} and 3*d*_{3/2} of Mo⁶⁺, while the peaks observed at 231.9 and 235.0 eV can be typically indexed as Mo 3*d*_{5/2} and 3*d*_{3/2} of Mo⁵⁺ [30, 40]. The obtained results can be assigned to the Mo–O bond, which can be implied that the Ti atoms can be taken place by the Mo atom in the TiO₂ lattice [30, 40]. Additionally, this was also occurred by the reduction of Mo⁶⁺ to Mo⁵⁺ as

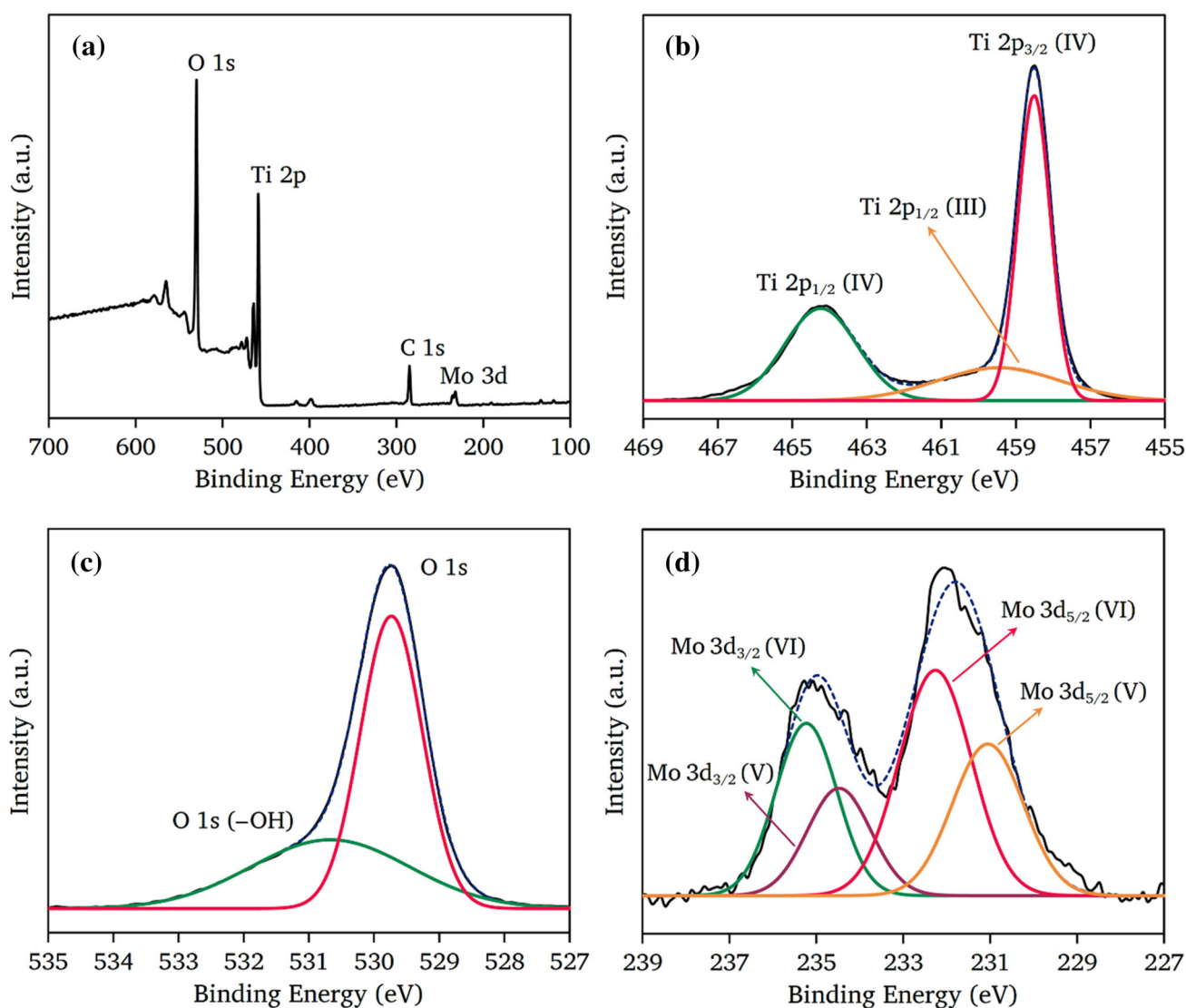


Fig. 4 Full-scale XPS spectra (a), the high-resolution XPS scan Ti 2*p* (b), O 1*s* (c), and Mo 3*d* (d) of 1.0% Mo:TiO₂ nanoparticles

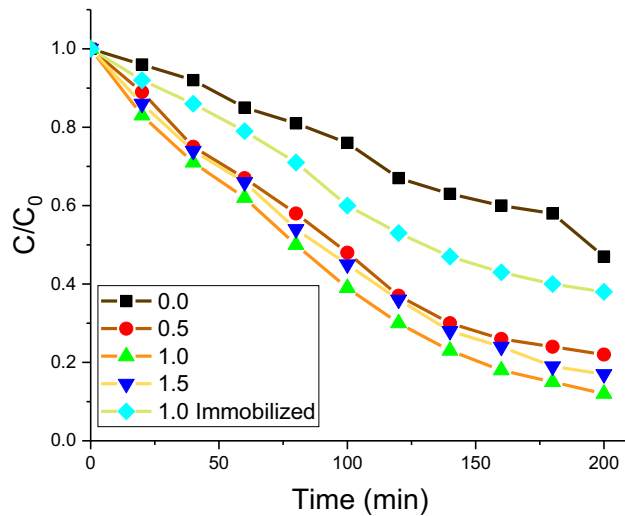


Fig. 5 Effect of dopant percentage on the photodegradation efficiency of humic acid

explained by Cui and co-workers [30]. What is more, Klosek and Raftery also reported a similar result that the appearance of V^{4+} in V-doped TiO_2 photocatalyst was due to the reduction of V^{5+} by Ti^{3+} generated in the calcination process [43].

3.2 Photodegradation of humic acid

3.2.1 Effect of doping percentage and immobilization of nanoparticles on the sandblasted glass

To evaluate and compare the effect of weight percentage of molybdenum as dopant and immobilization on removal efficiency, the photodegradation of humic acid in the presence of pure TiO_2 nanoparticles and $Mo:TiO_2$ was assessed under constant conditions of the reaction medium as the concentration of humic acid is equal to 25 mg/l, nanoparticle dosage is equal to 1 g/l, and pH is equal to 7 against the sunlight for 200 min. Figure 5 shows that the photodegradation of humic acid using pure TiO_2 was 43% after 200 min, while this efficiency increased to 78 and 88% in the case of 0.5 and 1.0 wt% $Mo:TiO_2$ nanoparticles, respectively. Moreover, the efficiency decreased to 83% in the case of 1.5 wt% $Mo:TiO_2$ nanoparticles. Moreover, the removal efficiency was reduced to 63% for immobilized 1.0 wt% $Mo:TiO_2$ nanoparticles, which is higher compared with pure TiO_2 but less than 0.5 and 1.0 wt % $Mo:TiO_2$ nanoparticles in slurry

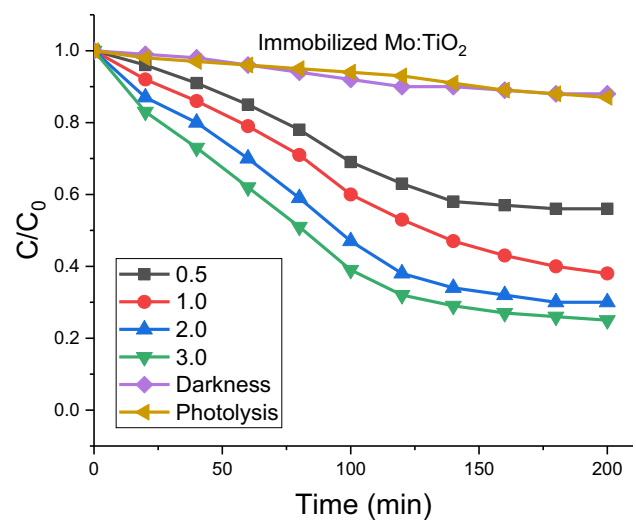
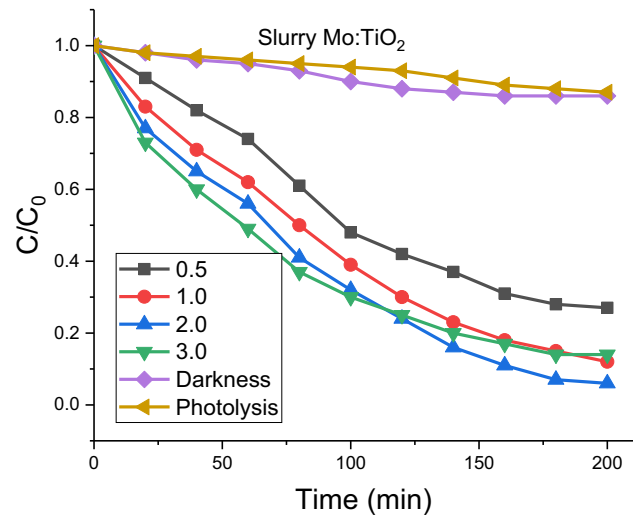


Fig. 6 Effect of $Mo:TiO_2$ dosage on the photodegradation efficiency of humic acid

mode. In any case, doping TiO_2 with Mo increased the photocatalytic degradation efficiency of humic acid compared with pure TiO_2 in the presence of sunlight. This can be due to the smaller ionic radius and band gap energy of Mo than TiO_2 , as well as reducing the rate of electron–hole recombination and ultimately increasing photocatalytic activity [28].

3.2.2 Effect of $Mo:TiO_2$ dosage on the photodegradation efficiency of humic acid

Figure 6 shows the effect of dosage (0.5, 1.0, 2.0, and 3.0 g/l) of 1.0% $Mo:TiO_2$ nanoparticles in slurry

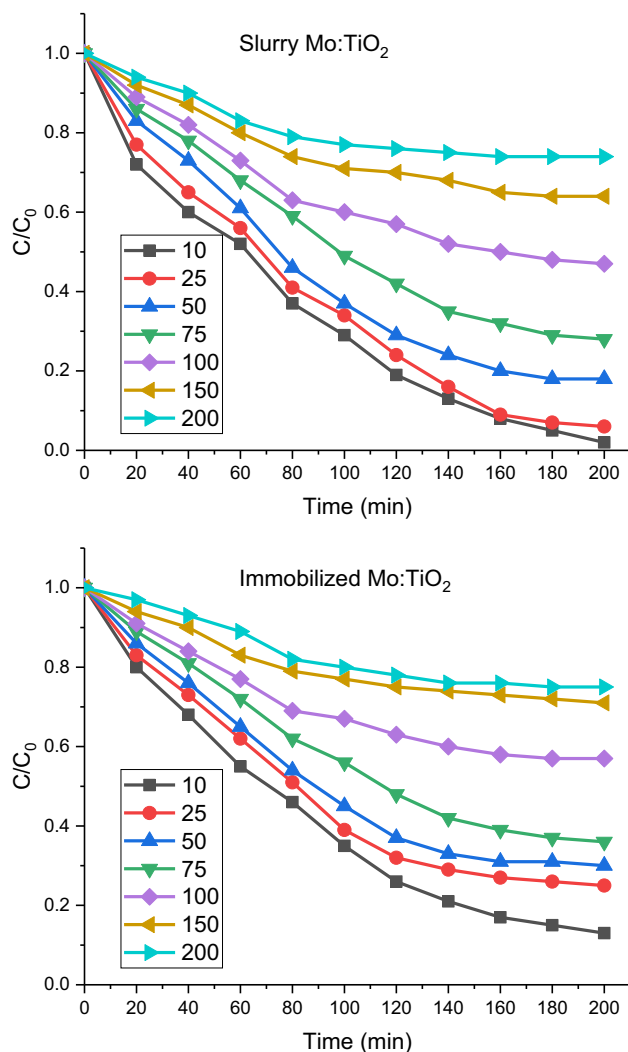


Fig. 7 Effect of humic acid concentration on its photodegradation efficiency (pH = 7; catalyst dosage 2 mg/l in the case of slurry and 3 g/100 ml in the case of immobilized)

mode and 1.0% immobilized Mo:TiO₂, with a base concentration of 0.5, 1.0, 2.0, and 3.0 g/100 ml of distilled water to cover the sandblasted glass, on the efficiency of photocatalytic degradation of humic acid under sunlight illumination. Moreover, degradation efficiency in the absence of a light source (in darkness) for both powder and immobilized Mo:TiO₂ was compared with the degradation efficiency in the presence of sunlight illumination without any materials (photolysis). The results showed that the degradation efficiency in both cases (catalyst without light source and light source without catalyst) was negligible. However, the removal efficiency of humic acid increased with the presence of a visible light source and photocatalyst. The maximum removal

efficiency of humic acid in the presence of 2 g/l Mo:TiO₂ nanoparticles in the slurry mode was 94% within 200-min contact time, while increasing the dosage of nanoparticles to 3 g/l, the degradation efficiency decreased to 86%. The reason for this trend can be attributed to the increase in the number of active sites available and the adsorption of more photons by increasing the number of nanoparticles. By adsorbing more light photons, more electrons are produced in the holes, resulting in more oxidizing radicals, and more pollutant decomposition occurs at the same time. The decreased photocatalytic efficiency of Mo:TiO₂ nanoparticles with higher loading of the catalyst can be attributed to higher dispersion and increased turbidity caused by nanoparticles and thus reduced penetration and contact of light photons with the catalyst surface [44, 45].

3.2.3 Effect of initial concentration of humic acid on its photodegradation efficiency

The effect of the initial concentration of humic acid on its photocatalytic degradation was evaluated by taking different concentrations (10 to 200 mg/l) of humic acid under constant reaction conditions of pH 7 and 2 g/l slurry Mo:TiO₂ nanoparticles and immobilized (3 g/100 ml coated on sandblasted glass) Mo:TiO₂ under sunlight illumination. According to the results presented in Fig. 7, the degradation efficiency decreased with increasing humic acid concentration in both processes, which can be attributed to several reasons. As the concentration of humic acid increases under steady-state conditions, more molecules of the pollutant are adsorbed on the active surfaces of the catalyst, thus reducing the production of the active hydroxyl and superoxide radical species and thus the degradation efficiency of the pollutant.

The introduction of Mo into the TiO₂ crystal structure subsequently creates a multi-band energy level (Fig. 8a) that tune the band gap energy toward the visible spectrum. The multi-band energy system within the TiO₂ structure enhances the photocatalytic activities under visible range and supports for continuous electron pathway that enhances the production of active radicals in an aqueous media. Continuous production of active radicals further initiates the degradation of humic acids and possible degradation pathways can be seen in Fig. 8b.

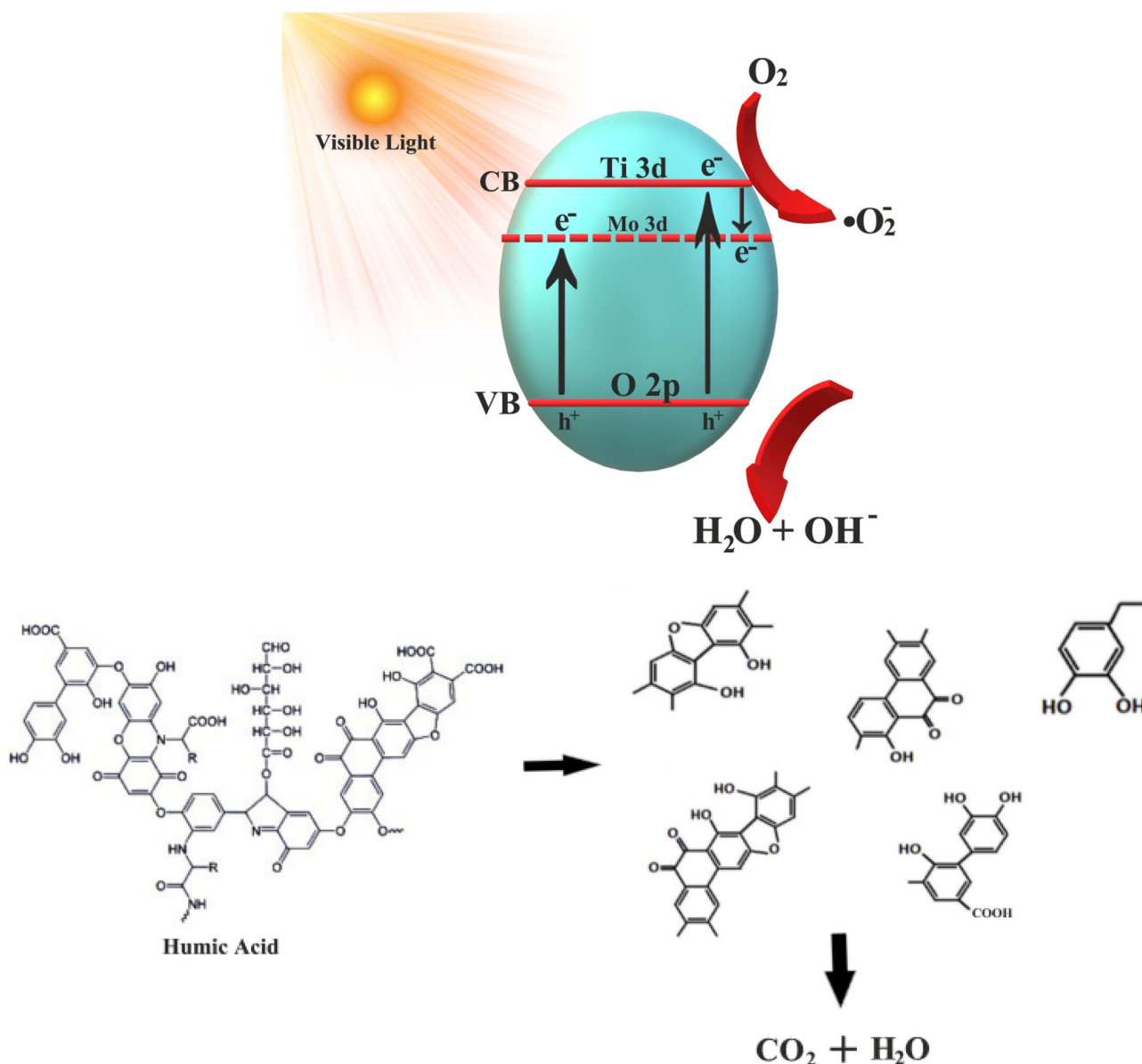


Fig. 8 Schematic band alignment of Mo:TiO₂ composite nanoparticles and possible degradation reaction of the humic acid molecules in the photocatalysis process

3.2.4 Photocatalytic stability test

The effect of the reusability of slurry and immobilized Mo:TiO₂ nanoparticles on the photodegradation efficiency of humic acid is depicted in Fig. 9. The photodegradation efficiency reduction after each run was less in slurry mode compared with immobilized Mo:TiO₂ nanoparticles so that after three times recycling this reduction reached 27 and 12% in the case slurry and immobilized mode, respectively. Such difference could be attributed to the release of nanoparticles as no substrate was used in slurry case.

Therefore, immobilization could be considered as an alternative for slurry mode. In addition, it is suggested to conduct ecotoxicity test for the nanoparticles used for photodegradation studies.

4 Conclusion

In this research work, Mo:TiO₂ nanoparticles were synthesized through the mild hydrothermal method. The fabricated nanomaterials had spherical morphology, showing excellent tailoring material for

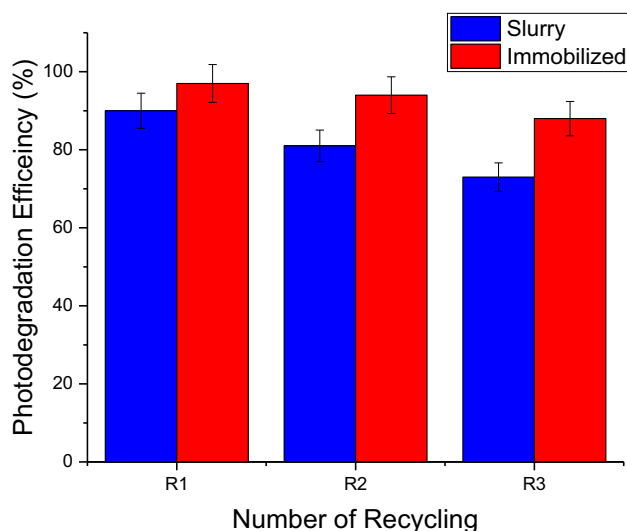


Fig. 9 Effect of recycling Mo:TiO₂ nanoparticles on the photodegradation of humic acid (pH = 7; catalyst dosage 2 mg/l in the case of slurry and 3 g/100 ml in the case of immobilized)

photodegradation. Doping with Mo increased photodegradation efficiency under both UV and sunlight.

Acknowledgements

This research was approved by the Ethic Committee of Kurdistan University of Medical Sciences (IRMUKREC. 1397/66). All the authors profusely thank the Kurdistan University of Medical Sciences, Sanandaj, Iran to have supported the review by providing the necessary access to electronic resources.

Author contributions

KA executed the laboratory experiments and prepared the first draft of the manuscript. KW, TS, and NA supported laboratory experiments and interpreted the results obtained. AM and SML contributed to interpretation, proofreading, and manuscript finalizing. BS and HPS directed and conceptualized the work and finally proofread the manuscript.

Funding

This research did not receive any specific grant from any funding agencies.

Data availability

All data generated or analyzed during this study are included in this published article.

Declarations

Conflict of interest None of the authors have any competing interests in the manuscript.

Ethical approval Not applicable.

Consent to participate Not applicable.

References

1. H. Kamani, S. Nasser, M. Khoobi, R. Nabizadeh Nodehi, A.H. Mahvi, Sonocatalytic degradation of humic acid by N-doped TiO₂ nano-particle in aqueous solution. *J. Environ. Health Sci. Eng.* **14**(1), 3 (2016). <https://doi.org/10.1186/s40201-016-0242-2>
2. M. Khodadadi, T.J. Al-Musawi, H. Kamani, M.F. Silva, A.H. Panahi, The practical utility of the synthesis FeNi₃@ SiO₂@ TiO₂ magnetic nanoparticles as an efficient photocatalyst for the humic acid degradation. *Chemosphere* **239**, 124723 (2020)
3. Á. de la Rubia, M. Rodríguez, D. Prats, pH, ionic strength and flow velocity effects on the NOM filtration with TiO₂/ZrO₂ membranes. *Sep. Purif. Technol.* **52**(2), 325–331 (2006)
4. E. Bazrafshan, H. Biglari, A.H. Mahvi, Humic acid removal from aqueous environments by electrocoagulation process using iron electrodes. *E-J. Chem.* **9**(4), 2453–2461 (2012)
5. A. Matilainen, M. Vepsäläinen, M. Sillanpää, Natural organic matter removal by coagulation during drinking water treatment: a review. *Adv. Colloid Interface Sci.* **159**(2), 189–197 (2010)
6. S. Moussavi, M. Ehrampoush, A. Mahvi, S. Rahimi, M. Ahmadian, Efficiency of multi-walled carbon nanotubes in adsorbing humic acid from aqueous solutions. *Asian J. Chem.* **26**(3), 821 (2014)
7. H. Rezaei, M.R. Narooie, R. Khosravi, M.J. Mohammadi, H. Sharafi, H. Biglari, Humic acid removal by electrocoagulation process from natural aqueous environments. *Int. J. Electrochem. Sci.* **13**(3), 2379–2389 (2018)
8. G. Asgari, A. Ebrahimi, A.S. Mohammadi, G. Ghanizadeh, The investigation of humic acid adsorption from aqueous solutions onto modified pumice with hexadecyl trimethyl ammonium bromide. *Int. J. Environ. Health Eng.* **2**(1), 20 (2013)

9. W.-W. Tang, G.-M. Zeng, J.-L. Gong, J. Liang, P. Xu, C. Zhang et al., Impact of humic/fulvic acid on the removal of heavy metals from aqueous solutions using nanomaterials: a review. *Sci. Total Environ.* **468**, 1014–1027 (2014)
10. M.N. Chong, B. Jin, C.W. Chow, C. Saint, Recent developments in photocatalytic water treatment technology: a review. *Water Res.* **44**(10), 2997–3027 (2010)
11. A. Jonidi-Jafari, M. Shirzad-Siboni, J.-K. Yang, M. Naimi-Joubani, M. Farrokhi, Photocatalytic degradation of diazinon with illuminated ZnO–TiO₂ composite. *J. Taiwan Inst. Chem. Eng.* **50**, 100–107 (2015)
12. R. Andreozzi, V. Caprio, A. Insola, R. Marotta, Advanced oxidation processes (AOP) for water purification and recovery. *Catal. Today* **53**(1), 51–59 (1999)
13. M. Shirzad Siboni, M.-T. Samadi, J.-K. Yang, S.-M. Lee, Photocatalytic removal of Cr (VI) and Ni (II) by UV/TiO₂: kinetic study. *Desalin. Water Treat.* **40**(1–3), 77–83 (2012)
14. M. Shirzad Siboni, M. Samadi, J. Yang, S. Lee, Photocatalytic reduction of Cr (VI) and Ni (II) in aqueous solution by synthesized nanoparticle ZnO under ultraviolet light irradiation: a kinetic study. *Environ. Technol.* **32**(14), 1573–1579 (2011)
15. S. Dehghan, A.J. Jafari, M. FarzadKia, A. Esrafil, R.R. Kalantary, Visible-light-driven photocatalytic degradation of metalaxyl by reduced graphene oxide/Fe₃O₄/ZnO ternary nanohybrid: influential factors, mechanism and toxicity bioassay. *J. Photochem. Photobiol. A* **375**, 280–292 (2019)
16. A. Fakhri, S. Rashidi, I. Tyagi, S. Agarwal, V.K. Gupta, Photodegradation of erythromycin antibiotic by γ -Fe₂O₃/SiO₂ nanocomposite: response surface methodology modeling and optimization. *J. Mol. Liq.* **214**, 378–383 (2016)
17. M. Hazarika, I. Saikia, J. Das, C. Tamuly, M.R. Das, Biosynthesis of Fe₂O₃@ SiO₂ nanoparticles and its photocatalytic activity. *Mater. Lett.* **164**, 480–483 (2016)
18. D.-G. Kim, S.-O. Ko, Cu@ Fe₃O₄ core-shell nanoparticle-catalyzed oxidative degradation of the antibiotic oxytetracycline in pre-treated landfill leachate. *Chemosphere* **191**, 639–650 (2018)
19. A. Mohagheghian, K. Ayagh, K. Godini, M. Shirzad-Siboni, Enhanced photocatalytic activity of Fe₃O₄-WO₃-APTES for azo dye removal from aqueous solutions in the presence of visible irradiation. *Part. Sci. Technol.* **37**(3), 358–370 (2019)
20. N. Radhika, R. Selvin, R. Kakkar, A. Umar, Recent advances in nano-photocatalysts for organic synthesis. *Arab. J. Chem.* **12**(8), 4550–4578 (2019)
21. Z. Wang, M. Chen, J. Shu, Y. Li, One-step solvothermal synthesis of Fe₃O₄@ Cu@ Cu₂O nanocomposite as magnetically recyclable mimetic peroxidase. *J. Alloys Compd.* **682**, 432–440 (2016)
22. G. Zhao, Z. Mo, P. Zhang, B. Wang, X. Zhu, R. Guo, Synthesis of graphene/Fe₃O₄/NiO magnetic nanocomposites and its application in photocatalytic degradation the organic pollutants in wastewater. *J. Porous Mater.* **22**(5), 1245–1253 (2015)
23. S. Wu, H. Hu, Y. Lin, J. Zhang, Y.H. Hu, Visible light photocatalytic degradation of tetracycline over TiO₂. *Chem. Eng. J.* **382**, 122842 (2020)
24. L. Chen, C. Zhao, D.D. Dionysiou, K.E. O’Shea, TiO₂ photocatalytic degradation and detoxification of cylindrospermopsin. *J. Photochem. Photobiol. A* **307**, 115–122 (2015)
25. S. Balachandran, N. Prakash, K. Thirumalai, M. Muruganandham, M. Sillanpää, M. Swaminathan, Facile construction of heterostructured BiVO₄–ZnO and its dual application of greater solar photocatalytic activity and self-cleaning property. *Ind. Eng. Chem. Res.* **53**(20), 8346–8356 (2014)
26. S. Banerjee, D.D. Dionysiou, S.C. Pillai, Self-cleaning applications of TiO₂ by photo-induced hydrophilicity and photocatalysis. *Appl. Catal. B* **176**, 396–428 (2015)
27. A. Akyol, M. Bayramoğlu, Photocatalytic degradation of remazol red F3B using ZnO catalyst. *J. Hazard. Mater.* **124**(1–3), 241–246 (2005)
28. C. Sajan, B. Shahmoradi, H. Shivaraju, K.L. Rai, S. Ananda, M. Shayan et al., Photocatalytic degradation of textile effluent using hydrothermally synthesised titania supported molybdenum oxide photocatalyst. *Mater. Res. Innov.* **14**(1), 89–94 (2010)
29. M.A. Behnajady, N. Modirshahla, M. Mirzamohammady, B. Vahid, B. Behnajady, Increasing photoactivity of titanium dioxide immobilized on glass plate with optimization of heat attachment method parameters. *J. Hazard. Mater.* **160**(2–3), 508–513 (2008)
30. M. Cui, S. Pan, Z. Tang, X. Chen, X. Qiao, Q. Xu, Physicochemical properties of nn heterostructured TiO₂/Mo–TiO₂ composites and their photocatalytic degradation of gaseous toluene. *Chem. Speciat. Bioavailab.* **29**(1), 60–69 (2017)
31. B. Shahmoradi, S. Yavari, Y. Zandsalimi, H. Shivaraju, M. Negahdari, A. Maleki et al., Optimization of solar degradation efficiency of bio-composting leachate using Nd: ZnO nanoparticles. *J. Photochem. Photobiol. A* **356**, 201–211 (2018)
32. B. Shahmoradi, I. Ibrahim, N. Sakamoto, S. Ananda, T. Guru Row, K. Soga et al., In situ surface modification of molybdenum-doped organic–inorganic hybrid TiO₂ nanoparticles under hydrothermal conditions and treatment of pharmaceutical effluent. *Environ. Technol.* **31**(11), 1213–1220 (2010)
33. J. Abdi, M. Yahyanezhad, S. Sakhaie, M. Vossoughi, I. Alemzadeh, Synthesis of porous TiO₂/ZrO₂ photocatalyst derived from zirconium metal organic framework for degradation of organic pollutants under visible light irradiation. *J. Environ. Chem. Eng.* **7**(3), 103096 (2019)

34. C. Howard, T. Sabine, F. Dickson, Structural and thermal parameters for rutile and anatase. *Acta Crystallogr. B* **47**(4), 462–468 (1991)
35. Y. Zhao, C. Li, X. Liu, F. Gu, H. Jiang, W. Shao et al., Synthesis and optical properties of TiO₂ nanoparticles. *Mater. Lett.* **61**(1), 79–83 (2007)
36. S. Ravi, F.W. Shashikanth, Magnetic properties of Mo-doped TiO₂ nanoparticles: a candidate for dilute magnetic semiconductors. *Mater. Lett.* **264**, 127331 (2020)
37. K.B. Koozegar, M. Mousaei, Synthesis and investigation of optical and photocatalytic properties of ZnO nanoparticles codoped with Ti/Si. *J. New Mater.* **8**(4), 71–81 (2018)
38. T. Suwannaruang, J.P. Hildebrand, D.H. Taffa, M. Wark, K. Kamonsuangkasem, P. Chirawatkul, K. Wantala, Visible light-induced degradation of antibiotic ciprofloxacin over Fe–N–TiO₂ mesoporous photocatalyst with anatase/rutile/brookite nanocrystal mixture. *J. Photochem. Photobiol. A* **391**, 112371 (2020). <https://doi.org/10.1016/J.JPHOTOCHEM.2020.112371>
39. T. Suwannaruang, P. Kidkhunthod, N. Chanlek, S. Soontaranon, K. Wantala, High anatase purity of nitrogen-doped TiO₂ nanorice particles for the photocatalytic treatment activity of pharmaceutical wastewater. *Appl. Surf. Sci.* **478**, 1–14 (2019). <https://doi.org/10.1016/J.APSUSC.2019.01.158>
40. D. Xue, J. Luo, Z. Li, Y. Yin, J. Shen, Enhanced photoelectrochemical properties from Mo-doped TiO₂ nanotube arrays film. *Coatings* **10**(1), 75 (2020). <https://doi.org/10.3390/COATINGS10010075>
41. B. Bharti, S. Kumar, H.-N. Lee, R. Kumar, Formation of oxygen vacancies and Ti³⁺ state in TiO₂ thin film and enhanced optical properties by air plasma treatment. *Sci. Rep.* **6**, 32355 (2016)
42. X. Ma, P. Tang, D. Liu, J. Zhang, L. Feng, L. Wu, Interface engineering of perovskite solar cells with air plasma treatment for improved performance. *Chem. Phys. Chem.* **18**(20), 2939–2946 (2017)
43. S. Klosek, D. Raftery, Visible light driven V-doped TiO₂ photocatalyst and its photooxidation of ethanol. *J. Phys. Chem. B* **105**(14), 2815–2819 (2002). <https://doi.org/10.1021/JP004295E>
44. S.R. Mirmasoomi, M.M. Ghazi, M. Galedari, Photocatalytic degradation of diazinon under visible light using TiO₂/Fe₂O₃ nanocomposite synthesized by ultrasonic-assisted impregnation method. *Sep. Purif. Technol.* **175**, 418–427 (2017)
45. P. Pascariu, I.V. Tudose, M. Sucheana, E. Koudoumas, N. Fifer, A. Airinei, Preparation and characterization of Ni, Co doped ZnO nanoparticles for photocatalytic applications. *Appl. Surf. Sci.* **448**, 481–488 (2018)

Publisher's Note Springer Nature remains neutral with regard to jurisdictional claims in published maps and institutional affiliations.